

# Record $I_{on}$ (0.50 mA/ $\mu$ m at $V_{DD}$ = 0.5 V and $I_{off}$ = 100 nA/ $\mu$ m)

## 25 nm-Gate-Length ZrO<sub>2</sub>/InAs/InAlAs MOSFETs

S. Lee<sup>1</sup>, V. Chobpattana<sup>2</sup>, C.-Y. Huang<sup>1</sup>, B. J. Thibeault<sup>1</sup>, W. Mitchell<sup>1</sup>, S. Stemmer<sup>2</sup>, A. C. Gossard<sup>2</sup>, and M. J. W. Rodwell<sup>1</sup>

<sup>1</sup>ECE Department, <sup>2</sup>Materials Department, University of California, Santa Barbara, CA 93106 USA,

Email: [sanghoon\\_lee@ece.ucsb.edu](mailto:sanghoon_lee@ece.ucsb.edu)

**Abstract:** We report MOSFETs with 25-nm gate length ( $L_g$ ), extremely thin 2.5 nm InAs channels and 0.7/3.0 nm (physical) Al<sub>2</sub>O<sub>x</sub>N<sub>y</sub>/ZrO<sub>2</sub> gate dielectrics, and 12 nm In<sub>0.53</sub>Ga<sub>0.47</sub>As vertical spacers in the raised epitaxial source/drain. The FETs establish key new DC performance records, at VLSI-relevant gate lengths (25 nm), including 0.50 mA/ $\mu$ m on-current (at 100 nA/ $\mu$ m  $I_{off}$  and 0.5 V  $V_{DD}$ ) and 77 mV/dec. subthreshold swing ( $SS$ ) at  $V_{DS}=0.5$  V. At 1  $\mu$ m  $L_g$  and  $V_{DS}=0.1$  V, the minimum subthreshold swing is 61 mV/dec., a record low for InAs/InGaAs, indicating high interface quality.

**Introduction:** InAs/InGaAs MOSFETs can provide large on-currents at low voltages, and are being investigated for VLSI application [1]-[9]. Yet, impact ionization, band-band tunneling, and source/drain (S/D) tunneling leakage currents can be high because of low bandgaps and low electron effective mass;  $I_{on}$  (at specified low  $I_{off}$  and  $V_{DD}$ ), has not previously surpassed Si. Here we report 25 nm- $L_g$  ZrO<sub>2</sub>/InAs/InAlAs MOSFETs with performance surpassing prior III-V MOSFETs [1]-[8] and comparable to, or surpassing, leading 20-25 nm  $L_g$  Si fin- [10] and nanowire [11] FETs. In these FETs, leakage currents are reduced, without substantially increasing the S/D pitch, by vertical InGaAs spacers in the raised regrown S/D [5], and by thin (2.5 nm) InAs channels for increased channel bandgap. The thin 0.7/3.0 nm (physical) Al<sub>2</sub>O<sub>x</sub>N<sub>y</sub>/ZrO<sub>2</sub> gate dielectrics [12], and the thin 2.5 nm channel together improve electrostatics, while the increased gate-channel capacitance arising from these thin layers offsets the loss in transconductance  $g_m$  arising from the low mobility of the thin 2.5 nm InAs channel, with 2.38 mS/ $\mu$ m  $g_m$  achieved at 25 nm  $L_g$ . A record 0.50 mA/ $\mu$ m on-current (at  $I_{off}=100$  nA/ $\mu$ m and  $V_{DD}=0.5$  V) is achieved at a VLSI-relevant 25 nm  $L_g$ .

**Device Fabrication:** The epitaxial layer structure, grown on semi-insulating InP by solid-source MBE, has a 50 nm unintentionally doped (U.I.D) InAlAs buffer, a 250 nm 1.0×10<sup>17</sup> cm<sup>-3</sup> P-type doped InAlAs barrier, a 100 nm U.I.D InAlAs barrier, a 2 nm 1.0×10<sup>12</sup> cm<sup>-2</sup> N-type InAlAs pulse-doped layer, a 5 nm U.I.D InAlAs setback, a 3.5 nm InAs (strained) channel and 2 nm of the U.I.D In<sub>0.53</sub>Ga<sub>0.47</sub>As spacer. To form 12-1000 nm long dummy gates, ~20 nm of HSQ was spun and patterned by e-beam lithography. To form the remainder of the vertical spacer and the N+ S/D, 10 nm U.I.D (~1.2×10<sup>15</sup> cm<sup>-3</sup>) and 60 nm Si-doped (4.0×10<sup>19</sup> cm<sup>-3</sup>) In<sub>0.53</sub>Ga<sub>0.47</sub>As were selectively regrown by MOCVD. Device mesas were isolated by wet-etch. The dummy gates were stripped in buffered HF, and ~2 nm of the In<sub>0.53</sub>Ga<sub>0.47</sub>As cap and ~1 nm of InAs channel were removed in the gate region by a 2-cycle isotropic digital etch [13], leaving a 2.5 nm InAs channel. The sample was then immediately loaded into an ALD. After *in-situ* N<sub>2</sub> plasma/TMA treatment during which ~0.7 nm of Al<sub>2</sub>O<sub>x</sub>N<sub>y</sub> was formed [14], a ~3 nm ZrO<sub>2</sub> gate dielectric was deposited [12]. The sample was then annealed in forming gas at 400°C. Ni/Au gate and Ti/Pd/Au S/D metal contacts were deposited using thermal and e-beam evaporation,

respectively. Fig. 1 shows a device cross-sectional schematic. The FETs have  $L_g$  ranging from 18 nm to 1  $\mu$ m, where  $L_g$  is defined as the spacing between the edges of the regrown layer. The surfaces of the vertical spacer is also gated, thus the effective gate length is ~35 nm greater than  $L_g$ , given the spacer thickness and regrowth angle. Fig. 2 shows a top-down SEM image, taken before gate metal deposition, for a 25 nm- $L_g$  device. In a production VLSI device, the increase in minimum S/D contact pitch will be determined by the spacer and N+ thicknesses and the regrowth angle; if regrowth can be made vertical, the spacer will not increase minimum S/D pitch.

**Results and Discussions:** Fig. 3 shows transfer characteristics of a 25 nm- $L_g$  FET showing 2.38 mS/ $\mu$ m peak  $g_m$  at  $V_{DS}=0.5$  V and 0.5 mA/ $\mu$ m  $I_{on}$  at  $I_{off}=100$  nA/ $\mu$ m and  $V_{DD}=0.5$  V. Its subthreshold characteristics (Fig. 4) show 72 mV/dec. minimum SS ( $SS_{min}$ ) at  $V_{DS}=0.1$  V and 77 mV/dec. at  $V_{DS}=0.5$  V. Defined at  $I_D=1$   $\mu$ A/ $\mu$ m, its threshold voltage is -85 mV and drain induced barrier lowering (DIBL) is 76 mV/V. Output characteristics (Fig. 5) show 303  $\Omega$ - $\mu$ m on-resistance ( $R_{on}$ ) at  $V_{GS}=0.7$  V. Considering now a 1  $\mu$ m- $L_g$  device (Fig. 6), subthreshold characteristics show 61 mV/dec.  $SS_{min}$  at  $V_{DS}=0.1$  V, the lowest reported for any III-V MOSFET, and negligible DC hysteresis, both indicating a high-quality dielectric. Gate leakage (Fig. 6) normalized to the gate metal overlap area is <1 A/cm<sup>2</sup> at all measured bias conditions. Fig. 7 shows  $R_{on}$  as a function of  $L_g$ . The  $R_{on}$  extrapolated to zero  $L_g$  is 168  $\Omega$ - $\mu$ m ( $\pm 25 \Omega$ - $\mu$ m fitting error), which contains ~85  $\Omega$ - $\mu$ m total excess S/D resistance arising from the large 1.2  $\mu$ m S/G and G/D spacings (Fig. 7, inset). Absent these large contact spacings,  $g_m$  and  $I_{on}$  would be larger, and  $R_{on}$  lower. Fig. 8 shows peak  $g_m$  at  $V_{DS}=0.5$  V versus  $L_g$ , compared to published III-V MOSFETs. Despite low mobility in the 2.5 nm InAs channel, sub-40 nm- $L_g$  devices have > 2 mS/ $\mu$ m peak  $g_m$ , which we attribute to high gate-channel capacitance from the thin dielectric and channel. Comparing results in the published III-V literature, the devices here reported show the lowest  $SS_{min}$  at all  $L_g$  (Fig. 9) of any III-V MOSFETs, and exhibit the smallest DIBL at all  $L_g$  (Fig. 9) of any planar III-V MOSFETs. Fig. 11 benchmarks  $I_{on}$  at  $I_{off}=100$  nA/ $\mu$ m and  $V_{DD}=0.5$  V as a function of  $L_g$ . The devices show the highest  $I_{on}$  of any III-V MOSFET at a 0.5 V supply voltage. (note  $I_{off}$  in [3] is extrapolated, not measured)

**Conclusion:** We have demonstrated highly scaled ZrO<sub>2</sub>/InAs/InAlAs MOSFETs exhibiting records for key DC parameters. A FET with 25 nm- $L_g$  shows 0.5 mA/ $\mu$ m  $I_{on}$  at  $I_{off}=100$  nA/ $\mu$ m and  $V_{DD}=0.5$  V and 77 mV/dec.  $SS_{min}$  at  $V_{DS}=0.5$  V. At 1  $\mu$ m- $L_g$  and  $V_{DS}=0.1$  V,  $SS_{min}$  is 61 mV/dec., indicating a very high quality dielectric-semiconductor interface.

**Acknowledgement:** This work was supported by the SRC Non-classical CMOS Research Center (Task 1437.009). A portion of this work was done in the UCSB Nanofabrication facility, part of the NSF funded NNIN network and MRL Central Facilities supported by the MRSEC Program of the NSF under award No. DMR 1121053.

## References:

- [1] J. Lin *et al.*, IEDM, p. 421 (2013)
- [2] T.-W. Kim *et al.*, IEDM, p.425 (2013)
- [3] S. W. Chang *et al.*, IEDM, p.417 (2013)
- [4] S. Kim *et al.*, IEDM, p.429 (2013)
- [5] S. Lee *et al.*, APL, vol.103, p.233503 (2013)
- [6] D. H. Kim *et al.*, IEDM, p.761 (2012)
- [7] J. J. Gu *et al.*, IEDM, p.633 (2012)
- [8] M. Radosavljevic *et al.*, IEDM, p.319 (2009)
- [9] U.Singisetti *et al.*, EDL, vol.30, p.1128 (2009)
- [10] C.-H. Jan *et al.*, IEDM, p.44 (2012)
- [11] S. Bangsaruntip *et al.*, IEDM, p.526 (2013)
- [12] V. Chobpattana *et al.*, APL, unpublished
- [13] S. Lee *et al.*, IPRM (2012)
- [14] V. Chobpattana *et al.*, JAP 114, (2013)

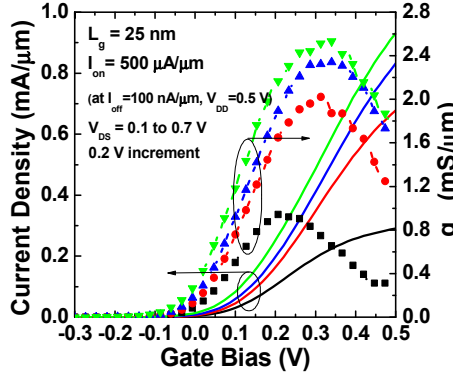


Fig. 3: Drain current  $I_D$  and transconductance  $g_m$ , versus  $V_{GS}$ , at 25 nm  $L_g$ .

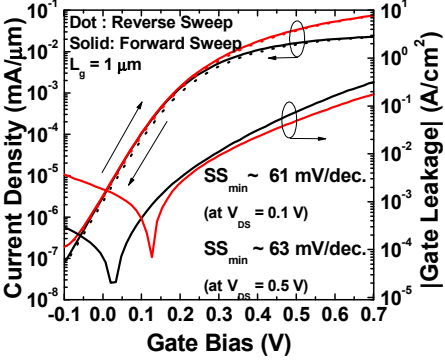


Fig. 6:  $\log(I_D)$  and  $\log(I_G)$  versus  $V_{GS}$ , at  $1 \mu\text{m} L_g$ , at  $V_{DS} = 0.1 \text{ V}$  and  $0.5 \text{ V}$ .

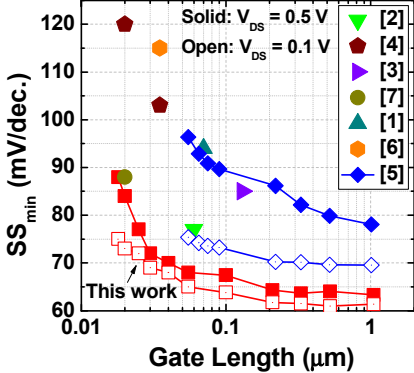


Fig. 9:  $SS_{min}$  as a function of  $L_g$ , compared to published III-V MOSFETs.

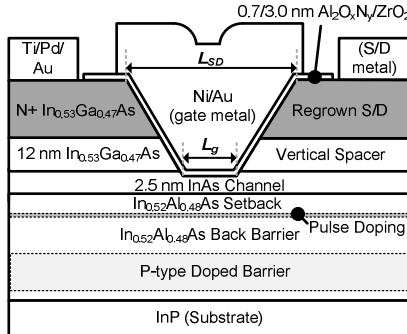


Fig. 1. Device schematic cross-section

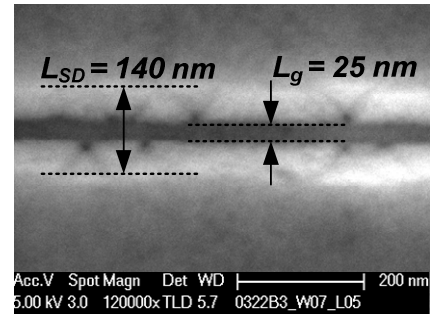


Fig. 2: SEM top-view image, before gate metal deposition, showing 25 nm  $L_g$ .

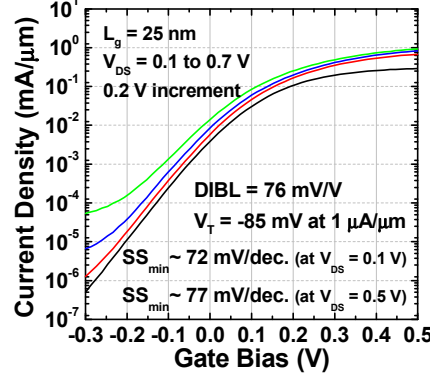


Fig. 4:  $\log(I_D)$  versus  $V_{GS}$ , at 25 nm  $L_g$ , at  $V_{DS} = 0.1, 0.3, 0.5$  and  $0.7 \text{ V}$ .

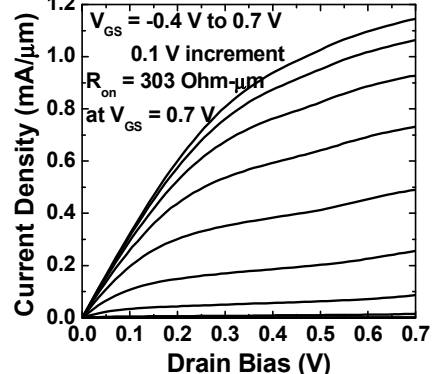


Fig. 5: Common-source DC characteristics at 25 nm  $L_g$ .

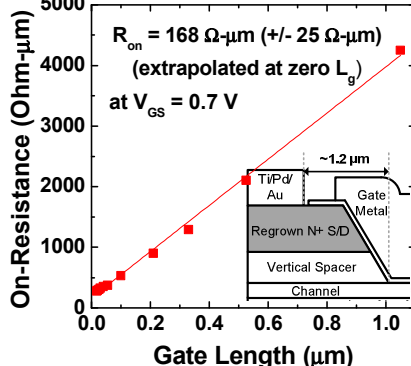


Fig. 7: Drain-source on-resistance versus  $L_g$ . The FETs have large S/G and G/D spacings.

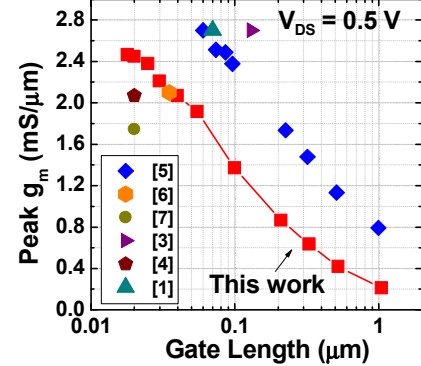


Fig. 8: Peak transconductance versus  $L_g$ , compared to the III-V literature.

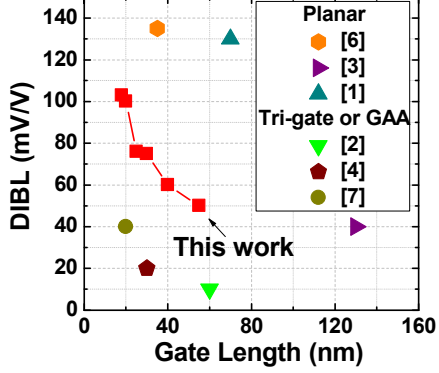


Fig. 10: DIBL as a function of  $L_g$ , compared to published III-V MOSFETs.

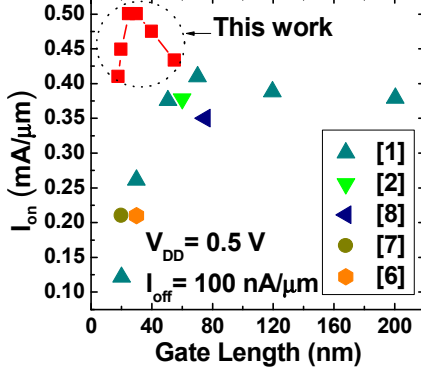


Fig. 11:  $I_{on}$ , at  $0.5 \text{ V}$   $V_{DS}$  and  $100 \text{nA}/\mu\text{m}$   $I_{off}$ , versus  $L_g$ , compared to the III-V literature.